

Non-resonant diagrams in radiative four-fermion processes

J. Fujimoto, T. Ishikawa, S. Kawabata, Y. Kurihara, Y. Shimizu ^a and D. Perret-Gallix ^b

^a Minami-Tateya Collaboration, KEK, Japan

^bLAPP-IN2P3/CNRS, France

The complete tree level cross section for $e^+e^- \rightarrow e^-\bar{\nu}_e u \bar{d} \gamma$ is computed and discussed in comparison with the cross sections for $e^+e^- \rightarrow e^-\bar{\nu}_e u \bar{d}$ and $e^+e^- \rightarrow \bar{u} d u \bar{d}$. Event generators based on the GRACE package for the non-radiative and radiative case are presented. Special interest is brought to the effect of the non-resonant diagrams overlooked so far in other studies. Their contribution to the total cross section is presented for the LEP II energy range and for future linear colliders ($\sqrt{s}=500$ GeV). Effects, at the W pair threshold, of order 3% ($e^-\bar{\nu}_e u \bar{d}$) and 27% ($\bar{u} d u \bar{d}$) are reported. Similar behaviour for the radiative case is shown. At $\sqrt{s}=500$ GeV, the relative contribution of the non-resonant diagrams for the radiative channel reaches 42.5%.

1. Introduction

Two years ago, a complete calculation of two four-fermion final states in e^+e^- collisions, $e^+e^- \rightarrow e^-\bar{\nu}_e u \bar{d}$ and $e^+e^- \rightarrow \bar{u} d u \bar{d}$, was reported at the Sochi meeting [1]. It was shown that the non-resonant diagrams play an important role below the W pair threshold (up to 27% at $\sqrt{s}=150$ GeV) and exhibit a non-negligible effect at higher energy (7% at $\sqrt{s}=190$ GeV). In these results, in addition to a set of experimental loose constraints, a cut on the θ angle of the outgoing electron was applied to cope with gauge violations appearing in the subset of $\gamma-W$ diagrams. Below threshold, the non-resonant diagrams competing only with the off-shellness of the resonant ones, their relative contribution becomes quite large. The non-resonant diagrams are dominated by t -channel $\gamma-W$ graphs in similarity with the well-known two-photon ($\gamma-\gamma$) processes. Hence the cross section increases with the energy and the contribution of non-resonant processes keeps growing in contrast to that of resonant diagrams which falls with the energy. This effect was confirmed at this workshop by the analysis of selected final states based on a dedicated four-fermion generator [2]. The non-resonant processes are essentially single W or no W production. Some examples of these type of diagrams for the radiative case can be seen on Fig.1b,2. As

far as the W mass reconstruction is concerned, these diagrams should be counted as background processes, and they will contribute to the overall mass and width measurement uncertainties.

It has been recognized, since some time [3], that the radiative corrections in W pair production have to be included for a precise comparison with measurements at the e^+e^- colliders. Initial state radiations (ISR) reduce the available center of mass energy. Close to the W pair threshold, ISR will, therefore, enhance the relative contribution of non-resonant diagrams. Final state radiative corrections will contribute to additional uncertainties on the mass reconstruction, unless the photon is detected and properly accounted for in the mass reconstruction algorithm. However, photons coming from the intermediate W, which can be mistakenly recognized as final state bremsstrahlung, will introduce additional uncertainties.

Although a number of studies has been carried out in these last years, including [4][5], we present, for the first time, the complete tree level computation of one of the radiative four-fermion processes. This work can be used as a benchmark for testing the validity of simplified and therefore faster generators.

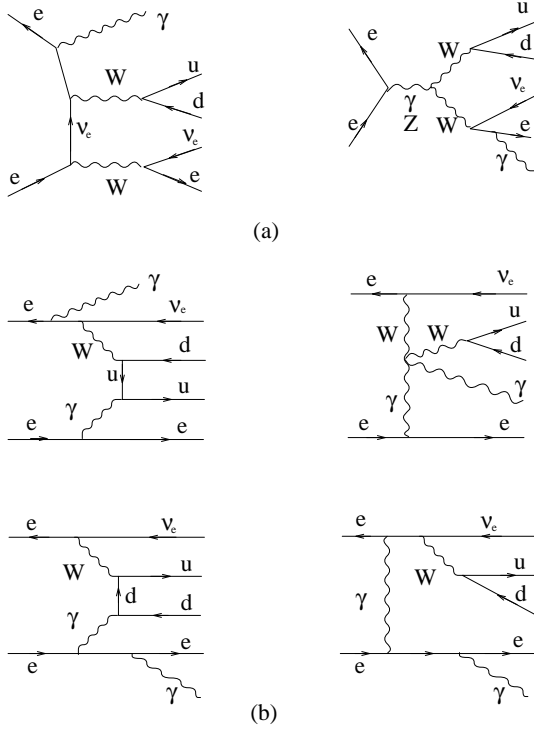


Figure 1. Some examples of diagrams from the radiative process $e^+e^- \rightarrow e^-\bar{\nu}_e u d \gamma$: a) Resonant diagrams, b) Non-resonant $\gamma - W$ diagrams.

2. The GRACE system

The GRACE system [6] has been used to perform the very lengthy computations involved in the study of most radiative processes. The GRACE package is a complete set of tools for computing tree level processes. All the phases involved in a given computation are covered: from the process definition (specification of the initial and final particles) to the event generator. It is composed essentially of three components: the diagram generator, the construction of the matrix element based on helicity amplitude function from the CHANEL [7] library and the multi-dimensional phase space integration package BASES [8] associated with the event generator SPRING [8].

Fermion masses are properly introduced in the helicity amplitudes. The particle width is introduced into the gauge boson propagators when

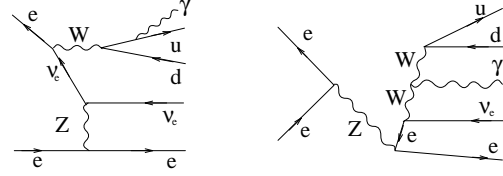


Figure 2. (Fig.1 cont.) Some examples of diagrams from the radiative process $e^+e^- \rightarrow e^-\bar{\nu}_e u d \gamma$: Other non-resonant diagrams.

the denominator can vanishes for positive squared momentum transfer. A gauge invariance checking program is automatically built by the system.

Only the kinematics for complex processes has to be written by the user. The issue, here, is to figure out what is the best transform to apply to the basic integration variables to regularize the divergencies appearing in the integration of the matrix element. The best kinematics will give the best accuracy for a given computation time.

3. Four-fermion production

The results presented hereafter have been obtained using the following set of parameters:

$$\begin{aligned}
 M_Z &= 91.1 \text{ GeV} \\
 \Gamma_Z &= 2.534 \text{ GeV} \\
 \alpha &= 1/137 \\
 \sin^2 \theta_W &= 1 - (M_W^2/M_Z^2) \\
 M_W &= 80 \text{ GeV} \\
 m_u &= m_d = 0.1 \text{ GeV}.
 \end{aligned}$$

The width of the W is taken from the Particle Data Table; $\Gamma_W = 2.25 \text{ GeV}$. The gauge boson (W,Z) widths are assumed to be constant in the calculation. Furthermore some realistic experimental cuts have been introduced:

$$\begin{aligned}
 \theta_e &> 8, 20, 30, 40^\circ \\
 172^\circ &> \theta_\gamma, \theta_{q,\bar{q}} > 8^\circ \\
 E_\gamma &> 1 \text{ GeV}, E_{e,q,\bar{q}} > 1 \text{ GeV}
 \end{aligned}$$

where θ_e, θ_γ and $\theta_{q,\bar{q}}$ are angles measured from the incident e^- beam and $E_{e,q,\bar{q}}$ are the energies of final e^-, q and \bar{q} , respectively. The electron

polar angle cut is introduced to avoid an undesirable gauge violation for extremely forward directions [9] caused inevitably by the finite width of W boson when the subset of $\gamma - W$ diagrams is considered.

The gauge invariance of the amplitude is checked numerically for a random selection of the boson gauge parameters at several points in the phase space. The errors are within the precision of numerical calculation (typically less than $O(10^{-12})$ in double precision) when the W width is turned off. Further gauge cancellations are checked to confirm that the obtained cross sections are stable against finite width. The procedure is as follows: first extract the product of gauge boson propagators without width as an overall factor of the whole amplitude. Then replace them by those with finite width. As a result, one is left with rigorously gauge invariant amplitude [10]. For the resonant diagrams, this method gives the same results as ordinal method. While for the $\gamma - W$ diagrams, this gives 10% smaller results.

3.1. The non-radiative case

The contribution of the non-resonant diagrams has been considered for two final states, $e^- \bar{\nu}_e u \bar{d}$ and $\bar{u} d u \bar{d}$. Fig.3 shows the cross sections versus the center of mass energy around the W pair threshold. The solid line represents the case where all diagrams are included, the dashed line the contribution of the resonant diagrams only. In the $\bar{u} d u \bar{d}$ channel, one can observe the onset of the Z resonant diagrams as a small shoulder starting around $2M_Z$. The behaviour below the W pair threshold can be better seen in fig.4 where the ratio of the three main resonant diagrams over the complete calculation is plotted for the same range of center of mass energy. In the $e^- \bar{\nu}_e u \bar{d}$ channel, the effect is of the order of $\pm 3\%$ around $\sqrt{s} = 160$ GeV, while in $\bar{u} d u \bar{d}$ it reaches -28% . At the energy of future LC, 500 GeV, the contribution of non-resonant diagrams is quite significant in $e^- \bar{\nu}_e u \bar{d}$ but is negligible in $\bar{u} d u \bar{d}$.

Similarly to the $\gamma - \gamma$ events, the non-resonant processes are predominantly peaked in the forward/backward direction. Fig.5 shows the behaviour of the cross section versus the electron

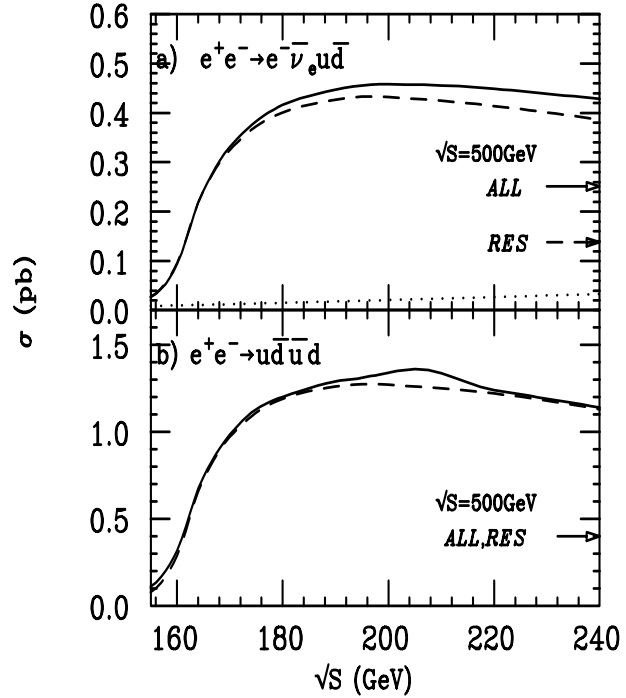


Figure 3. Cross sections for a) $e^+e^- \rightarrow e^- \bar{\nu}_e u \bar{d}$ and b) $e^+e^- \rightarrow \bar{u} d u \bar{d}$ versus C.M. energy with $\theta_e \geq 8^\circ$. The solid curves are for all diagrams and dashed ones for three resonant graphs. The dotted line in a) is the contribution from the $\gamma - W$ and $Z - W$ processes. The estimates at 500 GeV are indicated by arrows.

polar angle cut. The non-resonant contribution vanishes as the cut is raised.

3.2. The radiative case

In the covariant gauge, the GRACE package generates 752 diagrams when all the interactions are included, but actually 142 diagrams are used in the unitary gauge with Higgs-fermion coupling being set to 0. The full tree level computation requires, for a decent precision, some 100 hours on a HP 735 computer. Thanks to the vectorization of the integration package BASES, the most extensive computation could be performed on the KEK vector processor within 1 hour. Fig.6 shows the contribution of the non-resonant terms in the total cross section versus the C.M. energy. The behaviour is similar to the non-radiative case. In fig.7, one can see more clearly the contribution

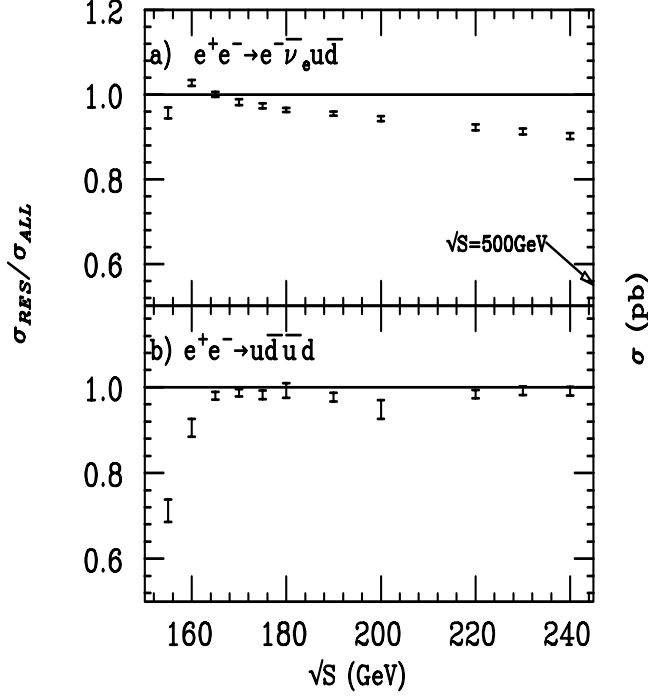


Figure 4. Energy dependence of the relative contribution of resonant diagrams in a) $e^+e^- \rightarrow e^-\bar{\nu}_e u \bar{d}$ and b) $e^+e^- \rightarrow \bar{u} d u \bar{d}$ with $\theta_e \geq 8^\circ$ to the full computation.

of non-resonant diagrams similar to fig.4 for non-radiative case.

The dependence of the cross section on the electron polar angle cut θ_e is presented in fig.8. Fig.9 shows the distribution of the invariant mass of the pairs of final state fermions. The general shape is, as expected, a Breit-Wigner distribution. However some background coming from the onset of non-resonant processes can be seen. In addition, for the radiative process (fig.10), a mass shift of the order of 1 GeV is observed on the $e^-\bar{\nu}_e$ invariant mass due to final state radiation.

4. Conclusions

A complete calculation of the radiative four-fermion final state $e^+e^- \rightarrow e^-\bar{\nu}_e u \bar{d} \gamma$ has been performed, for the first time, using automatic Feynman diagram calculation techniques implemented in the GRACE system. Comparison with

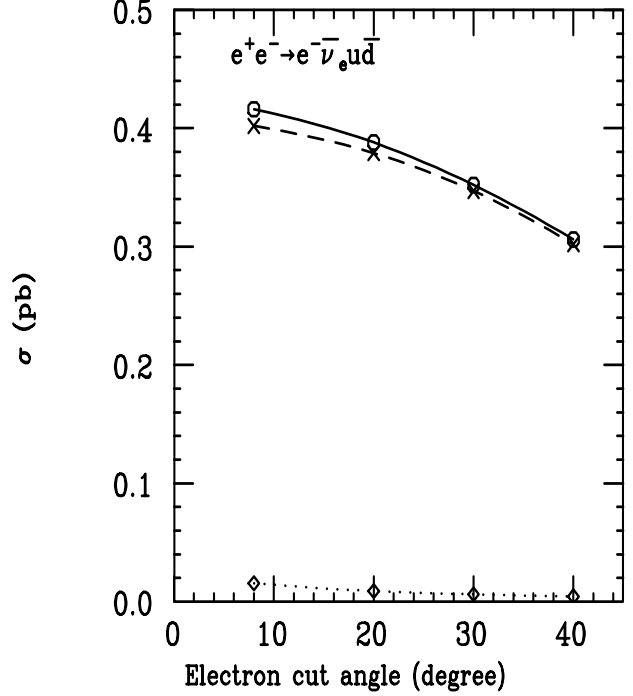


Figure 5. Electron angular cut dependence for $e^+e^- \rightarrow e^-\bar{\nu}_e u \bar{d}$ (C.M. energy = 180 GeV). Solid line: all diagrams, dashed line: three resonant diagrams and dotted line: $\gamma - W$ and $Z - W$ processes.

two non-radiative computations $e^-\bar{\nu}_e u \bar{d}$ and $\bar{u} d u \bar{d}$ has been carried out. The contribution of the non-resonant processes is large below threshold (at least for $\bar{u} d u \bar{d}$ channel) which makes the W mass determination from the excitation curve more difficult. At high energy, the contribution increases, reaching 46% ($e^-\bar{\nu}_e u \bar{d}$) and 42.5% ($e^-\bar{\nu}_e u \bar{d} \gamma$) at $\sqrt{s} = 500$ GeV. Determination of the W mass from direct reconstruction will have to deal with the intrinsic background from the non-resonant processes prominently in the forward direction. Furthermore the final state radiative correction will introduce a shift in the mass of the W unless the photon is properly taken into account in the algorithm of mass reconstruction. However, this last point may prove to be difficult as the photon may be produced either from the initial state, the intermediate charged boson or the final state fermions. Only this last class

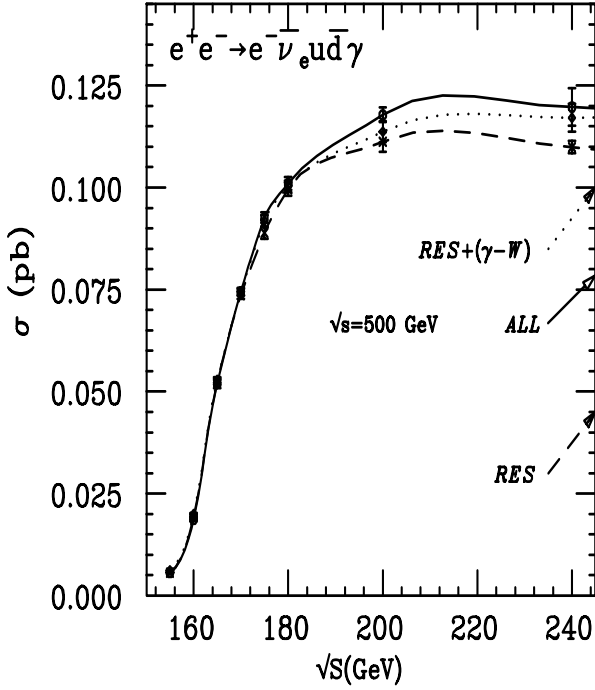


Figure 6. Total cross section for $e^+e^- \rightarrow e^-\bar{\nu}_e u\bar{d}\gamma$ versus the C.M. energy with $\theta_e \geq 8^\circ$. The solid line represents the complete cross section while the dotted line the resonant term only.

plays a role in the W mass determination. More detailed studies are needed to check if additional kinematical cuts can improve the mass determination.

However to quantify the actual relative contribution of radiative events in the total cross section, soft photon and one-loop contributions must be taken into account. Large negative contributions are expected, reducing, consequently, the number of radiative events and softening the mass reconstruction problem.

5. Acknowledgements

This work has taken place in the framework of the KEK-LAPP collaboration supported in part by the Ministry of Education, Science and Culture (Monbusho) under the Grant-in-Aid for International Scientific Research Program No. 04044158 in Japan and by le Centre National de

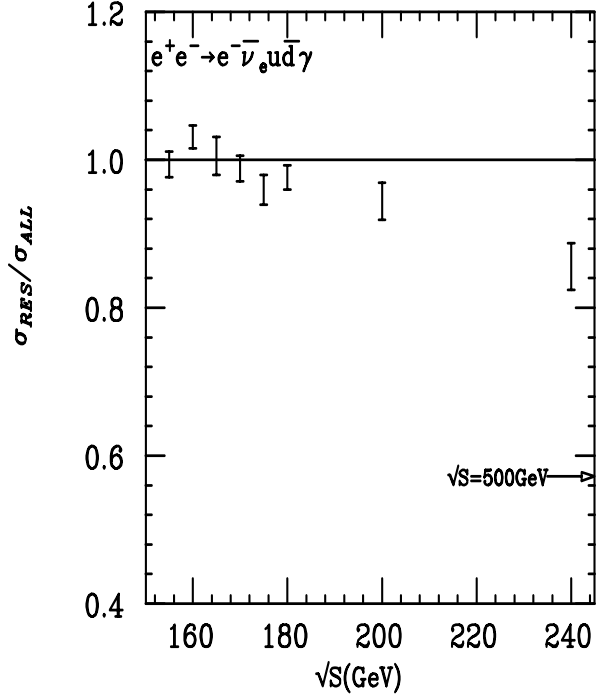


Figure 7. Energy dependence of the contribution of non-resonant diagrams in $e^+e^- \rightarrow e^-\bar{\nu}_e u\bar{d}\gamma$ with $\theta_e \geq 8^\circ$. The ratio of contribution of resonant diagrams versus all diagrams is shown.

la Recherche Scientifique (CNRS) and l'Institut de Physique Nucleaire et Physique des Particules (IN2P3) in France.

REFERENCES

1. T. Ishikawa, T. Kaneko, S. Kawabata, Y. Kurihara, Y. Shimizu and H. Tanaka, KEK Preprint 92-210, 1992 and in the *Proceedings of the 7th workshop on high energy physics and quantum field theory*, Sotchi, Russia, 1992.
2. M. Pittau, in these proceedings.
3. M. Lemoine and M. Veltman, *Nucl. Phys. B***164** (1980) 445
4. H. Tanaka, T. Kaneko and Y. Shimizu, *Comput. Phys. Commun.* **64**(1991) 149.
5. See related contributions in these proceedings.
6. T. Ishikawa, T. Kaneko, K. Kato, S. Kawa-

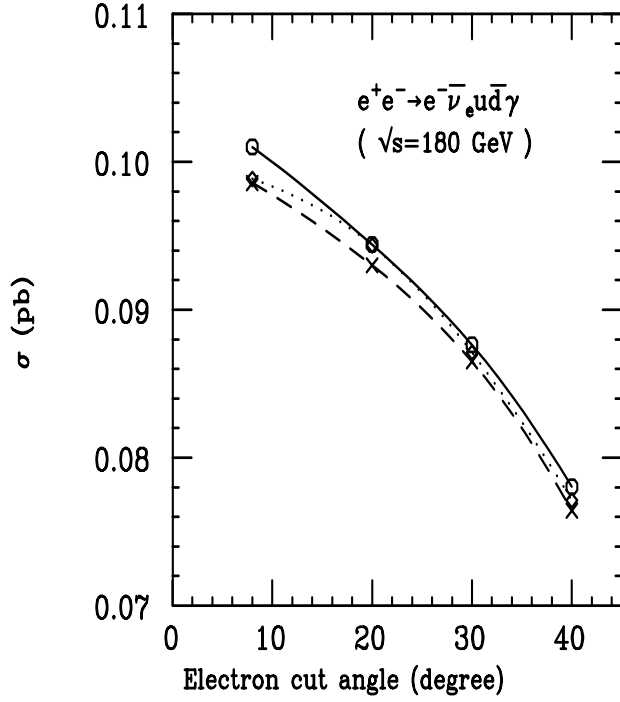


Figure 8. Total cross section for $e^+e^- \rightarrow e^- \bar{\nu}_e u \bar{d} \gamma$ versus the electron polar angle cuts in degree. The solid line: all diagrams, the dashed line: resonant diagrams, and the dotted line: resonant and $\gamma - W$.

- bata, Y. Shimizu and H. Tanaka, KEK Report 92-19, 1993, The Grace manual Ver. 1
7. H. Tanaka, *Comput. Phys. Commun.* **58** (1990) 153 and see also [4].
 8. S. Kawabata, *Comput. Phys. Commun.* **41**(1986) 127.
 9. E.E. Boos *et al.*, *Phys. Lett.* **B326**(1994) 190.
 10. A.E. Pukhov and V.A. Ilyin, private communication.

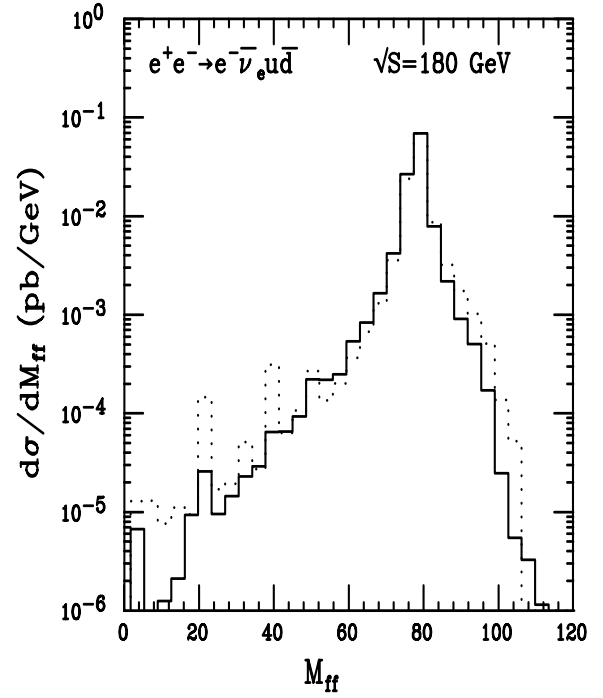


Figure 9. Invariant mass for non-radiative process in solid line for the $u \bar{d}$ system and in dotted line for the $e^- \bar{\nu}_e$ system with $\theta_e \geq 8^\circ$.

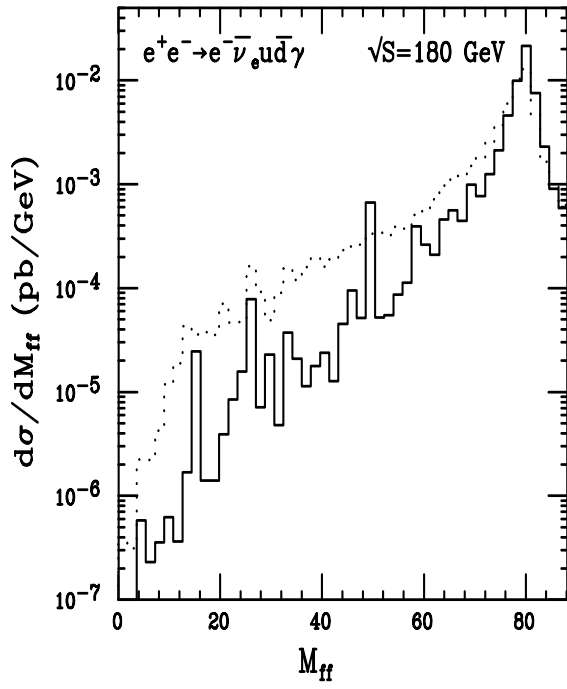


Figure 10. Invariant mass for radiative process in solid line for the $u\bar{d}$ system and in dotted line for the $e^-\bar{\nu}_e$ system with $\theta_e \geq 8^\circ$.